# CHARACTERIZING PANCREATIC CANCER SIGNALING, TOPOGRAPHY, AND CHEMOTHERAPEUTIC OUTCOMES WITH ORGANOID AND LIGHT-SHEET MICROSCOPIC THREE-DIMENSIONAL MODELS

Daniel Wilentz<sup>1</sup>, Bernat Navarro-Serer, Ph.D.<sup>2</sup>, Alexander Damanakis, M.D.<sup>2</sup>, Katherine Ganden<sup>1</sup>, Jennifer Gordinier<sup>1</sup>, and Laura D. Wood, M.D., Ph.D.<sup>2</sup>

Pine Crest School, Fort Lauderdale, FL<sup>1</sup> and Johns Hopkins University School of Medicine, Baltimore, MD<sup>2</sup>

### **Abstract**

Pancreatic cancer has a 5-year survival of just 10%, in part because it is aggressively invasive. Three-dimensional organoid cell cultures provide a way to investigate this invasion because they derive directly from patient tumors and maintain complex cellular interactions. Cancer-associated fibroblasts (CAFs) are the body's own cells that surround and influence cancers, often by producing extracellular signals. These experiments studied the interaction between CAFs and pancreatic cancer organoids and the impact of CAF signals on cancer invasion. Tumors were digested; cancer cells and CAFs from each tumor were sorted and cultured separately. After growing for 72 hours, CAFs were filtered out of their media, leaving only extracellular signals behind. CAF media was added to gels containing organoids derived from either the same patient or, most of the time, a different patient. Image analysis of the organoids was performed, and the circularity (roundness) of each image was traced with a Fiji picture-analysis system. While adding CAF media only slightly increased the percentage of invasive organoids, it significantly increased (p<0.05) the degree of invasiveness, as measured by the inverse of circularity. Importantly, this increased invasiveness was independent of whether the CAFs and cancers derived from the same patient or different patients. These data show that CAFs provide important, patient-independent extracellular signals influencing the invasiveness of pancreatic cancer. We now also have begun to build a database of three-dimensional computer images of resected pancreatic cancers derived from both control tumors and tumors treated with chemotherapy. Our expanding database of tumor images will be used to further understand the effects of chemotherapy on cancer shape and growth and specify areas of invasion for genetic study with the goal of developing treatments to block local and metastatic cancer spread.

# **Key Words**

Pancreatic ductal adenocarcinoma (PDAC)

Organoids

Cancer-Associated Fibroblasts (CAFs)

Circularity

Chemotherapy

Light-Sheet Microscopy

Three-dimensional Tumor Modeling

Sphericity

# Introduction

### In Vitro Pancreatic Cancer Models

Pancreatic cancer, primarily as pancreatic ductal adenocarcinoma (PDAC), is one of the deadliest malignancies with a low 5-year survival of just 10% (Sohn et al., 2000). In fact, pancreatic cancer is the third leading cause of cancer death in the United States. Over 60,000 people will be diagnosed this year with the disease, and about 50,000 patients will die (American Cancer Society, 2022). Pancreatic cancer has such a poor prognosis for two reasons: (1) it is often diagnosed very late in the course of the disease and (2) the cancer itself is inherently invasive, spreading easily into vessels and nerves (Sohn et al., 2000; Brat & Hruban, 1996).

There are many different models to study this invasiveness in the laboratory (Wood & Ewald, 2021). *Cell lines*, grown as monolayers, originally derive, sometimes long ago, from patient tumors. *Spheroids* are cell lines that are manipulated in the laboratory to grow in three dimensions. Scientists use *mouse models* to introduce mutations into the germlines of mice, and, as they age, these mice can develop tumors throughout their bodies similar to human cancers. When researchers transplant human tumors under the skin of immunocompromised mice, they create a *xenograft*; these xenografted tumors will grow to large sizes so they can be harvested and further studied. *Organoids* are intricate three-dimensional cultures made directly after digesting patient tumors and growing them in an extracellular matrix gel (Navarro-Serer & Wood, 2022). Table 1 outlines the advantages and disadvantages of all these different cancer model systems.

# **Pre-Clinical Organoid Models**

Organoid models have become a promising pre-clinical research tool for the interrogation of complex scientific questions, as they maintain three-dimensional structures and complex cell-cell interactions, while still allowing for gene editing. Therefore, experiments based on organoids can measure invasion patterns between control and treatment groups, which is the objective of this research; study the effects of adding genes into cancers through CRISPR; and compare the gene sequences of individual cancer cells (Wood & Ewald, 2021; Navarro-Serer & Wood, 2022; Boj et al., 2015; Driehuis et al., 2019; Huang et al., 2015; Huang et al., 2020; Moreira et al., 2017).

The purpose of this study focuses on organoid experimentation: using organoids to categorize degrees of invasion between treatment and control groups, in this case those treated and not treated with signals produced by cancer-associated fibroblasts (CAFs). CAFs are the most abundant type of cell in the pancreatic tumor microenvironment. While their most common function is to produce and remodel collagen, they also can suppress or promote tumor growth through recruiting blood vessels, establishing drug resistance, and impacting immune responses. However, the exact mechanism of these functions remains unknown (Chen & Song, 2019; Richards et al., 2017; Sahai et al., 2020).

In fact, scientists have discovered that there are different types of CAFs that surround cancers growing *in vivo* (see Figure 1). These include myCAFs (myofibroblastic CAFs), iCAFs (immune CAFs), and apCAFs (antigen-presenting CAFs) (Öhlund et al., 2017; Nurmik et al., 2020; Tsai et al, 2018). MyCAFs are those that most directly surround growing cancer cells, while iCAFs and apCAFs are located in the next layer, just beyond the myCAFs and the extracellular matrix that myCAFs produce. (The extracellular matrix is the background material in the body on which the CAFs and cancer cells grow).

While much is still not known about CAFs, each type of CAF appears to function differently, produce unique chemicals, and respond to distinct signaling pathways. For example, studies show that myCAFs usually lay down the extracellular matrix, respond to the TGF-E signaling pathway, and produce smooth-muscle actin, while iCAFs usually modulate the body's immune response, depend on the IL-1 signaling pathway, and release cytokines and chemokines (small molecules that attract immune and other cells to the area) (Öhlund et al., 2017; Nurmik et al., 2020; Tsai et al., 2018). Studies have shown that when grown *in vitro* in flasks, all CAFs differentiate almost exclusively into myCAFs; therefore, the research below, in which CAFs were grown in flasks, studies the interaction between pancreatic cancer organoids and the signals produced specifically by myCAFs (Pereira et al., 2017).

We aim to determine how CAFs impact pancreatic tumor invasion by using CAF-conditioned media on PDAC organoids grown in collagen I gels. If CAFs can help cancers grow *in vivo*, we hypothesize that adding media containing substances produced by CAFs to growing PDAC organoids will increase the invasive character of those PDAC organoids *in vitro*. This experiment will verify the utility of the CAF-PDAC organoid *in vitro* model in assessing and quantifying the relationship between CAF signals and pancreatic cancer invasion *in vivo*.

To investigate whether CAF signals from a different patient have a similar effect on invasion as those from the same patient, both matched (CAF media and PDAC organoids derived from the same patient) and unmatched (CAF media and PDAC organoids derived from two different patients) samples were used. Because only CAF signals (and not the CAF cells themselves producing the signals) are added to the organoid gels, we expect that adding CAF signals to organoids not only will increase the invasive character of the organoids but also will do so (and to a similar degree) in a manner independent of the origin of the CAF cells (that is, whether they are matched or unmatched).

The invasive character of the organoids will be assessed through an objective measurement known as circularity, which evaluates the "roundness" of the organoid. Circularity is a proven surrogate for the invasive character of an organoid, and it is calculated by the equation  $4\pi(A/P^2)$ , with A representing area and P representing perimeter (Rasband 2017). Organoids that are perfectly round (circularity=1) are completely

non-invasive. Those that have protrusions (pseudopods) "invading" into the surrounding gel have lower circularity values and higher invasive characters. The more protrusions an organoid has, the lower its circularity and the greater its invasiveness.

# **Experimental Methods**

The experiments occurred in two overall parts: (1) the creation of PDAC collagen I gels and CAF-conditioned media and (2) the analysis of PDAC organoid invasion (circularity assessment) after the addition of CAF-cleared media. All procedures described (1) followed biosafety guidelines established by the researching institution's Department of Health, Safety, and the Environment and (2) were previously approved by the research university's Institutional Review Board of the Office of Human Subjects Research.

### Materials

Scalpels, Collagenase II and dispase powders, Low-growth culture media, 10X DMEM media, NaOH, Collagen I, Ice, RPMI media, 2D flasks, 4% paraformaldehyde, Computer, Fiji Picture-Analysis Software, Prism Software

# Part 1: Creation of PDAC Collagen I Gels and CAF-Conditioned Media

As a result of the COVID pandemic, Part 1 of this research occurred within the laboratory of the primary investigator, with the student in observation mode when possible, connecting via Zoom. PDAC tumors derived from consented pancreatic cancer patients were harvested and digested mechanically and enzymatically (cut into very small fragments with scalpels; digested with a mix of collagenase and dispase powders at 37°C; shaken for 1.5-2h; filtered to remove undigested pieces). Cancer cells were embedded in collagen I gels (made by mixing 100  $\mu$ L culture media, 32 $\mu$ L NaOH, and 868  $\mu$ L collagen I, pH $^{\sim}$ 7; gel was incubated in ice for 15-20 min for polymerization), producing organoids within them. Organoids were then cultured overnight (about 16h) with a low-growth media. See Figure 2 for a diagram of the general procedure to make an organoid gel.

CAFs, previously sorted by flow cytometry from consented patient tumors, were grown in RPMI media in 2D flasks. After 72 hours, CAF-conditioned media was filtered (0.22 µm filter) to remove any cell debris (a total of 15 mL CAF-conditioned media was harvested). CAF-conditioned media was then added to organoids in collagen I gels (1:1 ratio, 800 µl of each). Each collagen gel contained organoids derived from a single patient, and each conditioned CAF media contained substances produced by CAFs also derived from a single patient. The CAF media and the organoid gel were "matched" if the CAF media and the organoid gel were each derived from the same patient; they were "unmatched" if the added CAF media and the organoid gel were from

different patients. Control groups were generated by adding RPMI media in which CAFs had never been grown to each collagen gel. Organoids were then cultured and allowed to invade for 3-4 days. After that, organoids were fixed with 4% paraformaldehyde, and images of at least 40 organoids from each gel were taken. See Figure 3 for an outline of the procedure to make CAF media and add it to an organoid gel.

# Part 2: Analysis of PDAC Organoid Invasion (Circularity) After Adding CAF-Cleared Media

As a result of the COVID pandemic, part 2 of this project took place at the student's home with the student using a computer to work virtually and independently, with subsequent reviews with the supervising scientist.

Multiple organoids originally derived from four different patient tumors (B161, B164, B165, and B173) were treated with control or CAF media (CAF2, CAF3, CAF4, or CAF5) and their invasion was analyzed. There were forty organoids examined for each organoid gel-CAF media pairing; therefore, 800 different organoids (4 patients X 5 control or CAF media X 40 organoids per pairing) were examined. Although the tumors and CAF media were designated with different codes, the tumors and CAF media originated in the same set of patients; for example, B151 and CAF2 represented an organoid and CAF media sample that, before manipulation in the laboratory to produce the organoids and the CAF media, were both harvested from the same patient's tumor at the time of surgery. Therefore, when organoid gel B161 was co-cultured with CAF2 media, the samples in this trial were "matched" (i.e., they originated from same patient); however, when B161 was treated with CAF3, CAF4, or CAF5, the samples were "unmatched" (i.e., the CAF media added to B161 organoids was from one of the other patients).

Over 800 organoids in all these different matched and unmatched pairings were observed and subjected to both time-lapse and still-frame photography. See Figure 4 for a diagram summarizing the origin of these 800 organoids derived from cancers from 4 patients and treated with both matched and unmatched CAF media.

Time-lapse photography of the organoids was performed. The circularity of each organoid was traced using a Fiji picture-analysis system. Circularity provides an objective measurement of organoid invasiveness: perfect circularity=1.0; circularity<1 signifies increased invasiveness.

To analyze each organoid, the Fiji program was opened, and the image of the organoid was dragged into the program. After choosing "Polygon Selection" within the Tools Menu, the organoid was enlarged by placing the cursor in the middle of the organoid and clicking the plus (+) key on the keyboard. If necessary, an organoid was minimized with the minus/dash (-) button. The operator can zoom in or out of each organoid at any time to facilitate analysis. The initiation analysis point in the organoid was created by clicking the mousepad. The operator traveled around the organoid border with clicks at regular intervals until coming back

to the initiation point. The operator saved the image as a Tiff file by first clicking File, then Save As, and finally Tiff.

The circularity measurement (Circ.) was displayed, and the measurement was pasted into an Excel spreadsheet. If there were multiple organoids in a single image, all of the organoids were analyzed. Each organoid was saved in a file with an extra suffix of 1, 2, or 3, depending on the order in which that particular organoid was analyzed. Circularity values were tabulated, analyzed, and graphed with Prism software, a statistical program. The Prism software performs one-way ANOVA and Kruskal-Wallis statistical tests on the samples, depending on whether the results follow a normal distribution curve (use one-way ANOVA) or do not (use Kruskal-Wallis). The statistical tests can establish whether the difference in circularity values between the control and treatment groups is significant.

# Results

Qualitatively, non-invasive organoids maintained their roundness (circularity), while those becoming invasive developed protrusions infiltrating into the surrounding gel. Figure 5 shows an example of a relatively non-invasive organoid, compared to an invasive one.

To make an objective comparison of the degree of invasiveness observed in all of the photographs similar to those in Figure 5, circularity values were calculated for each organoid. The photographs of all of the organoids from each paired organoid-CAF set were placed in a designated folder, and the tracing of each organoid was replicated either two or three times. If the first two replicated measurements produced values differing by less than 0.1, the two values were averaged to determine the reported circularity value. If instead the measurements differed by 0.1 or greater, a third measurement was taken, and the average of the two closest measurements was reported as the final circularity value. The contour of each organoid was traced out using the Fiji picture-analysis software (see Materials and Methods). Figure 6 shows the successive tracing of an organoid image in order to arrive at a circularity value. Figure 7 demonstrates completed circularity tracings for two samples from the same patient, one treated with control media and one treated with unmatched CAF media.

While adding CAF media to the organoid gels only slightly increased the *number* of invasive organoids, it statistically significantly increased the *degree* of invasiveness among all of the collectively invasive organoids (p<0.05, one-way ANOVA). Overall, the percentage of invasive organoids among organoids treated with a CAF media was 46%, while the percentage of invasive organoids among those subjected only to control media was 36% (not significant, one-way ANOVA). In contrast, the overall average circularity value among organoids treated with a CAF media was 0.548, while the average circularity value among organoids bathed only with control media was 0.735 (p<0.0001, one-way ANOVA). Because invasion and circularity are inversely related,

we believe it is actually more intuitive to compare the *inverse* of the circularity values between these two groups, with the higher inverse circularity value signifying a higher level of organoid invasiveness: inverse circularity for the control group was 1/0.735, or 1.36, while that for the treatments groups was 1/0.548, or 1.82 (p<0.0001, one-way ANOVA).

The data therefore confirm the hypothesis that the CAF secretome increases the degree of invasion among PDAC organoids. An analysis of the data also demonstrates that PDAC organoid invasiveness is independent of the patient origin of the CAFs with respect to the organoid. The matched samples had similar percentages of invasive organoids and circularity values as the unmatched samples (matched: 47% invasive, 0.542 average circularity value, 1.85 average inverse circularity; unmatched: 46% invasive, 0.551 average circularity value, 1.81 average inverse circularity). There was no significant difference in any of these values between the matched and unmatched treated organoid groups (one-way ANOVA). The signals from CAFs increased the invasive nature of the PDAC organoids, as measured by their loss of circularity, whether or not the CAFs originated in the same patient or a different patient as the PDAC organoid did.

Both of these phenomena are best demonstrated in Figure 8, which uses patient B161 as an example (patient's B161 matched CAF sample is CAF2). On the left graph in the figure, the number of invasive organoids increases with the addition of CAF media (whether matched or unmatched, from CAF2, CAF3, CAF4, or CAF5, indicated by "+" in the CAF chart below the bars in columns 2-5), but that increase is not statistically significant ("ns"; one-way ANOVA), compared to the number of invasive organoids treated with the control media (first column, no CAF media added, all "-" values in the CAF chart below the bar graph). However, the right graph of this figure shows that the *degree* of invasiveness, as measured by the inverse of the circularity, between the untreated organoids (first column) and the treated organoids (last four columns) *is* statistically significant (p<0.0001, one-way ANOVA).

# **Discussion and Conclusion**

The data in these experiments support our original hypothesis that the addition of CAF media to pancreatic cancer organoids increases their invasive nature, but this manipulation does so only in *degree* and not by number (see Results data and Figure 8). Among the treatment (CAF-conditioned media added) and control groups, there is no significant difference in the percentage of organoids that become invasive. However, there is a significant difference in degree of invasion, as measured by inverse of circularity, between these groups. We thus show that circularity  $(4\pi(A/P^2))$  is indeed a direct and objective way to measure the invasiveness of an organoid in culture. In summary, these results show that CAFs provide important extracellular signals

influencing the invasiveness of PDACs and that this *in vitro* organoid model can be used as a surrogate for CAF-cancer signaling within the body.

In addition, the influence of these signals is not restricted by the patient origin of the CAFs (see Results data and Figure 8). CAFs derived from a different patient had the same effect on pancreatic organoid invasion as did CAFs derived from the same patient as the organoids. Hence, we can conclude that while a patient's pancreatic cancer is different genetically from another patient's tumor, the CAFs recruited by each of these tumors may be more similar than the cancers, at least in terms of their signaling profiles. We can also surmise that although cancers are different from one another, they are alike in that each tumor finds a way to recruit the host's CAFs to its location; these recruited CAFs then can behave in similar ways with respect to influencing that cancer, regardless of the exact genetic makeup of that cancer.

Some shortcomings of this study include the limited number of patients from which the organoids in it were derived and the possibility of imprecision and inaccuracy in measuring the organoids via the tracing program. Although many (over 800) organoids were photographed and traced, these organoids and also the CAF media with which they were treated originated from only four patients; it will be important to expand these studies to more patients to see if the results continue to hold. In addition, while the organoid tracings in this study were replicated twice and even three times if necessary, they were performed by one person; it would also be helpful to have two people tracing out the organoids independently and a third observer re-tracing out any organoids in which there was significant disagreement in the circularity values produced by the two original measurers. Both of these experimental modifications will help verify and expand our results.

Our studies, as with most scientific exploration, leads to more questions in this field. For example, in our experiments, the CAFs were grown under normoxic ("normal oxygen") conditions. However, in the body, tumors grow in very hypoxic (oxygen-deprived) microenvironments. Further studies will investigate the effects of hypoxia on the relationship between organoid invasion and CAF signaling; CAF media and organoid gels each can be produced under both hypoxic and normoxic conditions, and the effects of mixing these different conditions on circularity values can be determined. In addition, as described above, CAFs are not uniform, and they come in three subcategories (Öhlund et al., 2017; Nurmik et al., 2020; Tsai et al., 2018). Since all of the CAFs in our experiments had differentiated into myCAFs by virtue of growing the CAFs in a flask (see Introduction), it would also be interesting to repeat these experiments for each CAF type (myCAF, iCAF, and apCAF) and compare the results. CAFs can be forcibly differentiated into each of these subcategories under specific growth and signaling conditions (Öhlund et al., 2017; Nurmik et al., 2020; Tsai et al., 2018).

While studying pancreatic cancer invasion with laboratory cultures is extremely informative, it is also important to examine the actual behavior of the disease *in vivo*. This is accomplished by examining and characterizing cancers removed from a patient at the time of surgery. Currently, tissue obtained during surgery is cut into small pieces, fixed in formalin, and embedded in a paraffin block. Histotechnologists cut two-dimensional slices of the tumor from the block and press it onto a glass slide. The glass slide is stained with the chemicals hematoxylin and eosin (H&E), and a pathologist examines the stained slide (Westra & Phelps, 1996).

By examining these very thin slices of tumor under the microscope, the pathologist verifies the diagnosis of cancer and recognizes specific properties of it, including its type (based on what part of the pancreas the tumor resembles); its differentiation (how closely the tumor mimics that part of the pancreas); and its invasion into vessels, nerves, and surrounding tissue (Vincent et al., 2011). Knowing the tumor type, differentiation, and invasive pattern of a cancer are important because they help predict the tumor's prognosis (Zhao & Liu, 2020).

While routine H&E sections provide essential information about each tumor examined, they have significant limitations. First, slides stained with only H&E are sometimes difficult to interpret. Pancreatic cancers are often poorly differentiated, which means that the tumor cells grow as single cells and can hide within the background of normal pancreatic cells. Identifying invasion of the tumor into vessels and nerves, both important prognostic factors, can be challenging for the same reason. Pathologists also often have trouble distinguishing between cancer and non-cancerous conditions, such as chronic pancreatitis, when using only H&E staining (Kleeff et al., 2016).

The solution to many of these problems with routine H&E staining is the use of immunohistochemistry. Immunolabeling is the process by which portions of a tissue are highlighted with specific antibodies that attach to areas of interest, separating out these tissue components for easy visualization (Noë et al., 2018). For example, the antibody cytokeratin 19 stains normal pancreatic ducts and cancerous pancreatic tissue, while CD31 stains normal and cancerous blood vessels (Jain et al., 2010; Pusztaszeri et al., 2006). Because cytokeratin 19 antibodies stain cancers and the ducts of the normal pancreas, and not the rest of the normal pancreas (containing acini and islets of Langerhans), it can be used to understand the relationship between normal pancreatic ducts and cancerous pancreatic tissue growing around it.

The routine slides examined in a diagnostic laboratory have another problem, especially when there is a goal to best understand a cancer's invasion pattern. Since each routine slide captures only a two-dimensional picture of a very thin slice of a tumor, it is not possible to fully see the shape of the tumor or the pattern of its invasion into blood vessels, nerves, and surrounding normal tissues. While this information may not be necessary in the daily practice of pathology, three-dimensional imaging in mouse models with various gene

knock-outs provide a way to better understand tumor growth and thus how cancers like PDAC react to their environments (Hessmann et al., 2020).

The easiest way to create a three-dimensional model of a human pancreatic cancer is to combine the technique of immunolabeling with three-dimensional light-sheet imaging (Strack, 2021; Keller & Dodt, 2012). The three-dimensional light-sheet microscope works with a laser moving across each of the three dimensions of a cube of tissue and examining a cross section at each level (Keller & Dodt, 2012). The immunolabeling highlights areas in different colors depending on the antibody and chromogen used, and a computer analyzing light-sheet microscope images batches these images based on the colors detected. The computer then stacks all of the cross sections on top of one another and creates a three-dimensional model (Noë et al., 2018; Liu et al., 2020).

The information from three-dimensional imaging provides valuable information on tumor growth and invasion. By observing how tumors invade native vessels and nerves, it may be possible to determine the means by which tumors are first able to spread beyond the pancreas. This information could lead researchers to develop ways to block this initial access to the rest of the body, thereby either preventing or slowing pancreatic cancer's invasiveness and increasing its survival rate. Three-dimensional imaging can also provide information on the effects of chemotherapy on tumor progression (Hong et al., 2019). Differences in tumor load and location after chemotherapy can help investigators understand the mechanism and effectiveness of different chemotherapeutic treatments.

# Materials and Methods for Light-Sheet Microscopy

### Materials

Multiple Samples of Paraffin-Embedded Human Cancer Tissue (previously resected and de-identified), Methanol, Distilled  $H_20$ , Mixers,  $H_2O_2$ , PBS, DMSO, Triton X, Donkey Serum, CD31 Antibody, CK19 (cytokeratin 19) Antibody, Secondary Anti-CD31 and -CK19 Antibodies, SUMIC, Isopropyl Alcohol, DCM, DBE, Light-sheet Microscope, LabKit Imaging Software

# Methods

This research took place "after" the COVID pandemic and was performed in-person at the downtown Baltimore and Homewood campuses of Johns Hopkins University. Previously resected, paraffin-embedded pancreatic tumors were permeabilized for and stained with immunohistochemical markers, rendered transparent with a tissue-clearing protocol, examined with a light-sheet microscope, and converted into three-dimensional

computerized images. Gloves, masks, and a fume hood were used when performing experiments with all hazardous materials. All chemicals were placed in labeled disposal containers after use.

An approximately 3 x 3 x 3-mm sample of a pancreatic tumor was removed from a de-identified tissue block originally produced for pathologic study at the time of pancreatic resection. This tissue sample was dehydrated with successive MeOH:distilled  $\rm H_20$  washes, each with 1 mL of liquid for 20 minutes on a mixer set for 70 rotations/minute (wash 1: 50%:50% MeOH:H<sub>2</sub>0, wash 2: 80%:20% MeOH:water, washes 3 and 4: 100% MeOH). The solution was decanted after each wash. Each sample was then bleached with 300  $\mu$ l  $\rm H_2O_2$  and 1550  $\mu$ l MeOH and incubated for 3 hours at room temperature. The tissue was then rehydrated with washes identical to the dehydration procedure but in reverse sequence.

To permeabilize the tissue for upcoming immunohistochemistry, it was washed three times with 1 ml of PBS (20 minutes and at 70 rotations/minute) and incubated overnight at 4C. A mixture of collagenase II and PBS (1:4 ratio, 1000µl in total) was added to the tumor and was rotated at 180 rotations/minute on a mixer for 30 minutes. The tumor was again washed with PBS twice for 5 minutes each time and stored overnight at 4C.

Immunohistochemistry was performed on the appropriately prepped tissue. First, a block solution of PBS (860 μL), DMSO (100 μL), Triton X (5 μl), and donkey serum (20μL) was prepared and incubated for 20 minutes 37C. The now-permeabilized tumor and two primary antibodies (10 μL of CD 31 and 5 μL of cytokeratin [CK] 19) were added to the Eppendorf tube containing the block solution. The CD31 antibody targets vessels, while CK19 stains cancerous glands. These antibodies preferentially label their targets because they specifically recognize their antigen partners, which are only (or more) expressed on the tissue types where the antibodies attach (Vincent et al., 2011; McKenney & Hornick, 2018; McKenney & Hornick, 2020). The mixture was then incubated overnight at 4C. The following day, eight SUMIC washes were performed: four times for 15 minutes and four more times for 30 minutes. Secondary antibodies, each containing a chromagen (2 μL of anti-CD31 antibody: red; 1 μL of anti-CK19 antibody:green), were added to the tumor in the tubes. The solution was kept overnight at 4C, and the eight SUMIC washes were performed again the next morning.

Because light-sheet microscopy examines cross-slices of 3-mm thick pieces of tissue, the tissue must be cleared, or made see through, so that light can pass through it and be read by the microscope (Vincent et al., 2011). To do so, the tissue was successively dehydrated with 30%:70% isopropyl alcohol:water, 50%:50% isopropyl alcohol:water, 80%:20% isopropyl alcohol:water, and 100% isopropyl alcohol (the last step repeated three times), each for 30 minutes on a mixer (70 rotations/minute). The tissue was delipidized twice with 1ml of 100% DCM for 30 minutes on a mixer (70 rotations/minute). Finally, after a wash with 100% DBE, the tumor was stored at 4°C for future use in light-sheet microscopy, when thousands of cross-sectional photos were taken. LabKit imaging software compiled the photos together into a three-dimensional model, and parameters can be

set within the program to analyze tumor location, size, and shapes in individual or groups of tumors (e.g., those treated and untreated with previous chemotherapy protocols).

# **Light-Microscopy Results and Discussion: Ongoing Analysis**

We have created computer models of six pancreatic ductal adenocarcinomas. An example of one of these models after rendering with the LabKit software is shown in Figure 9. Because the fluorophore attached to the anti-CD31 and anti-CK19 antibodies were red and green, respectively, the red areas in the model represent vessels, while the green areas represent islands of cancer cells.

We have also begun to examine the effects of chemotherapy on these tumors. Preliminary data from three pancreatic cancers indicate that chemotherapy preferentially reduces cancer load inside vessels when compared to that at primary pancreatic sites. Figure 10 shows a tumor after treatment with the chemotherapeutic regimen gemcitabine/Abraxane, compared to a control tumor. The results have been similar in the three tumors examined thus far.

Finally, based on measurements of sphericity (which compares the surface areas of standardized spheres to those of cancerous glands), cancer cells from enlarging tumors primarily form tubules, not spheres (Figure 11). Because the LabKit program allows the tumors to be filtered according to the sphericity of the shapes within them, comparisons between the same tumor at different sphericity values can be made. When a sphericity value for an image is chosen, cancer cells with sphericity values above that setting disappear from view. Hence, if a tumor image set at a low sphericity value is very similar to the original image, most of the tumor contains cells with sphericities below that value. Because the images (original image versus one dialed for all cells with sphericities below 0.5) in Figure 11 significantly overlap, it can be assumed that most of the cancer cells in the figure form tubules (low sphericity), as opposed to spheres (high or perfect sphericity). This observation suggests that pancreatic cancer modifies its shape to optimize growth along native vessels, nerves, and ducts.

We continue to expand our database of tumors imaged with light-sheet microscopy with the aim of using them to further understand cancer invasion and specify areas of invasion for genetic study (e.g., transcriptomics) with the long-term goal of developing treatments to block local and metastatic cancer spread.

# References

- American Cancer Society. (2022).
   <a href="https://www.cancer.org/cancer/pancreatic-cancer/about/key-statistics.html">https://www.cancer.org/cancer/pancreatic-cancer/about/key-statistics.html</a>.
- 2. Boj, S.F., Hwang, C.I., Baker, L.A., et al. (2015). Organoid models of human and mouse ductal pancreatic cancer. *Cell.* Jan 15; 160(1-2):324-38.
- 3. Brat, D.J. & Hruban, R.H. (1996). Images in clinical medicine. A metastasis caught in the act. *N Engl J Med.* Dec 5; 335(23): 1733.
- 4. Chen, X. & Song, E. (2019). Turning foes to friends: targeting cancer-associated fibroblasts. *Nat Rev Drug Discov*. Feb; 18(2):99-115.
- 5. Driehuis, E., van Hoeck, A., Moore, K., et al. (2019). Pancreatic cancer organoids recapitulate disease and allow personalized drug screening. *Proc Natl Acad Sci USA*. Dec 9; 116(52):26580–90.
- 6. Hessmann, E., Buchholz, S. M., Demir, I. E., et al.. (2020). Microenvironmental determinants of pancreatic cancer. *Physiol Rev.* 100(4):1707–1751.
- 7. Hong, S.-M., Jung, D. J., Kiemen, A., et al. (2019). Three-dimensional visualization of cleared human pancreas cancer reveals that sustained epithelial-to-mesenchymal transition is not required for venous invasion. *Mod Pathol.* 33(4):639–647.
- 8. Huang, L., Holtzinger, A., Jagan, I., et al. (2015). Ductal pancreatic cancer modeling and drug screening using human pluripotent stem cell- and patient-derived tumor organoids. *Nat Med.* Nov; 21(11):1364-71.
- Huang, W., Navarro-Serer, B., Jeong, Y.J., et al. (2020). Pattern of Invasion in Human Pancreatic Cancer Organoids Is Associated with Loss of SMAD4 and Clinical Outcome. *Cancer Res.* Jul 1; 80(13):2804-2817.
- Jain, R., Fischer, S., Serra, S., et al. (2010). The use of Cytokeratin 19 (CK19) immunohistochemistry in lesions of the pancreas, gastrointestinal tract, and liver. *Appl Immunohistochem Mol Morphol*. Jan; 18(1): 9-15.
- 11. Keller, P.J., Dodt, H.U. (2012). Light sheet microscopy of living or cleared specimens. *Curr Opin Neurobiol*. Feb; 22(1):138-43.
- 12. Kleeff, J., Korc, M., Apte, M., et al. (2016). Pancreatic cancer. Nat Rev Dis Primers. Apr; 21(2): 16022.
- 13. Liu, S., Huh, H., Lee, S.H., et al. (2020). Three-Dimensional Single-Molecule Localization Microscopy in Whole-Cell and Tissue Specimens. *Annu Rev Biomed Eng.* Jun 4; 22:155-184.

- 14. McKenney, J.K., Hornick, J.L. (2018). Immunohistochemistry in Surgical Pathology. *Adv Anat Pathol*. Nov; 25(6): 373.
- 15. McKenney, J.K., Hornick, J.L. (2020). Immunohistochemistry in Surgical Pathology: Part 2. *Adv Anat Pathol.* May; 27(3): 113.
- 16. Moreira, L., Bakir, B., Chatterji, P., et al. (2017). Pancreas 3D Organoids: Current and Future Aspects as a Research Platform for Personalized Medicine in Pancreatic Cancer. *Cell Mol Gastroenterol Hepatol*. Dec 16; 5(3):289-298.
- 17. Navarro-Serer, B. & Wood, L.D. (2022). 3D organoids: the new tool to advance pancreatic cancer research. In preparation.
- 18. Noë, M., Rezaee, N., Asrani, K., et al. (2018). Immunolabeling of cleared human pancreata provides insights into three-dimensional pancreatic anatomy and pathology. *Amer J Pathol.* 188(7):1530–1535.
- 19. Nurmik, M., Ullmann, P., Rodriguez, F., et al. (2020). In search of definitions: Cancer-associated fibroblasts and their markers. *Int J Cancer*. Feb 15; 146(4):895-905.
- 20. Öhlund, D., Handly-Santana, A., Biffi, G., et al. (2017). Distinct populations of inflammatory fibroblasts and myofibroblasts in pancreatic cancer. *J Exp Med.* Mar 6;214(3):579-596.
- 21. Pereira, B.A., Vennin, C., Papanicolaou, M., et al. (2019). CAF Subpopulations: A New Reservoir of Stromal Targets in Pancreatic Cancer. *Trends Cancer*. Nov; 5(11):724-741.
- 22. Pusztaszeri, M.P., Seelentag, W., Bosman, F.T. (2006). Immunohistochemical expression of endothelial markers CD31, CD34, von Willebrand factor, and Fli-1 in normal human tissues. *J Histochem Cytochem*. Apr; 54(4): 385-95.
- 23. Rasband, W. (2017). <a href="https://imagej.nih.gov/ij/plugins/circularity.html">https://imagej.nih.gov/ij/plugins/circularity.html</a>.
- 24. Richards, K.E., Zeleniak, A.E., Fishel, M.L., et al. (2017). Cancer-associated fibroblast exosomes regulate survival and proliferation of pancreatic cancer cells. *Oncogene*. Mar 30; 36(13):1770-1778.
- 25. Sahai, E., Astsaturov, I., Cukierman, E., et al. (2020). A framework for advancing our understanding of cancer-associated fibroblasts. *Nat Rev Cancer*. Mar; 20(3):174-186.
- 26. Sohn, T.A., Yeo, C.J., Cameron, J.L., et al. (2000) Resected adenocarcinoma of the pancreas-616 patients: results, outcomes, and prognostic indicators. *J Gastrointest Surg.* Nov-Dec; 4(6): 567-79.
- 27. Strack, R. (2021) Single-objective light sheet microscopy. *Nat Methods*. Jan; 18(1):28.
- 28. Tsai, S., McOlash, L., Palen, K., et al. (2018). Development of primary human pancreatic cancer organoids, matched stromal and immune cells and 3D tumor microenvironment models. *BMC Cancer*.

- Mar 27; 18(1):335.
- 29. Vincent, A., Herman, J., Schulick, R., et al. (2011). Pancreatic cancer. *Lancet*. Aug 13; 378(9791): 607-20.
- 30. Westra, W.H., Phelps, T.H. (1996). Surgical Pathology Dissection: An Illustrated Guide, Volume 1. Springer.
- 31. Wood, L.D. & Ewald, A.J. (2021) Organoids in cancer research: a review for pathologist-scientists. *J Pathol.* Jul; 254(4):395-404.
- 32. Zhao, Z., Liu, W. (2020). Pancreatic Cancer: A Review of Risk Factors, Diagnosis, and Treatment. *Technol Cancer Res Treat.* Jan-Dec; 19:15.

# Figures and Tables

Model	Origin	Cost	3D Structure	Gene Editing	Co-Culture
Cell lines	Many passages (originally derived from human tissue)	Least expensive	No	Easiest	Possible
Spheroids	Cell culture	Expensive	No	Easy	No
Murine xenografts	Human tissue	Very expensive	Yes	Possible, but only before implantation	Limited
Engineered mice	Native mouse tumors	Very expensive	Yes	Possible, but requires extensive breeding	N/A
Organoids	Human tissue	Expensive	Yes	Possible, but can be challenging	Yes

**Table 1**. Advantages and Disadvantages of different laboratory cancer models. Adapted from (Navarro-Serer, 2020).

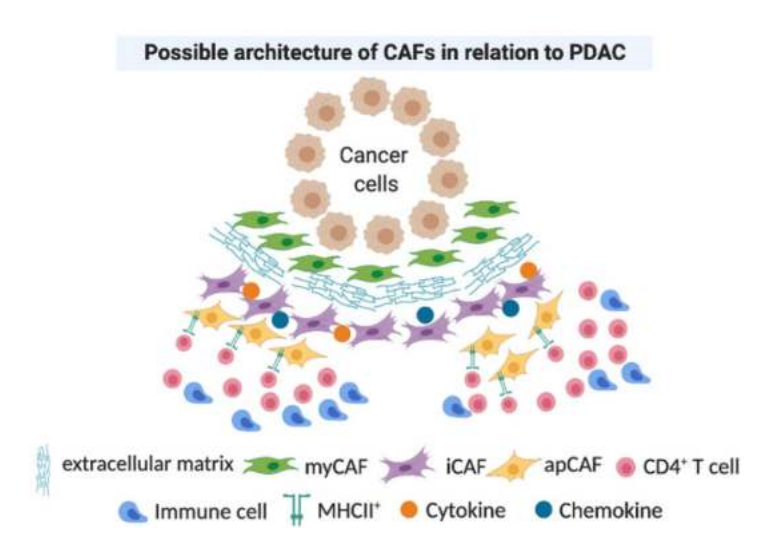


**Figure 1.** CAFs surround cancers and influence how they grow by producing signals that modulate blood vessel growth, drug resistance, and immune responses. Figure from (Öhlund, 2017).

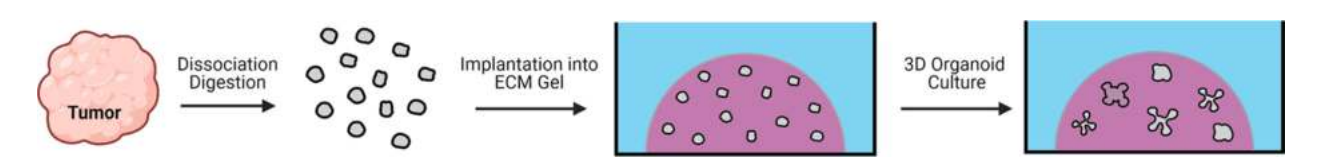
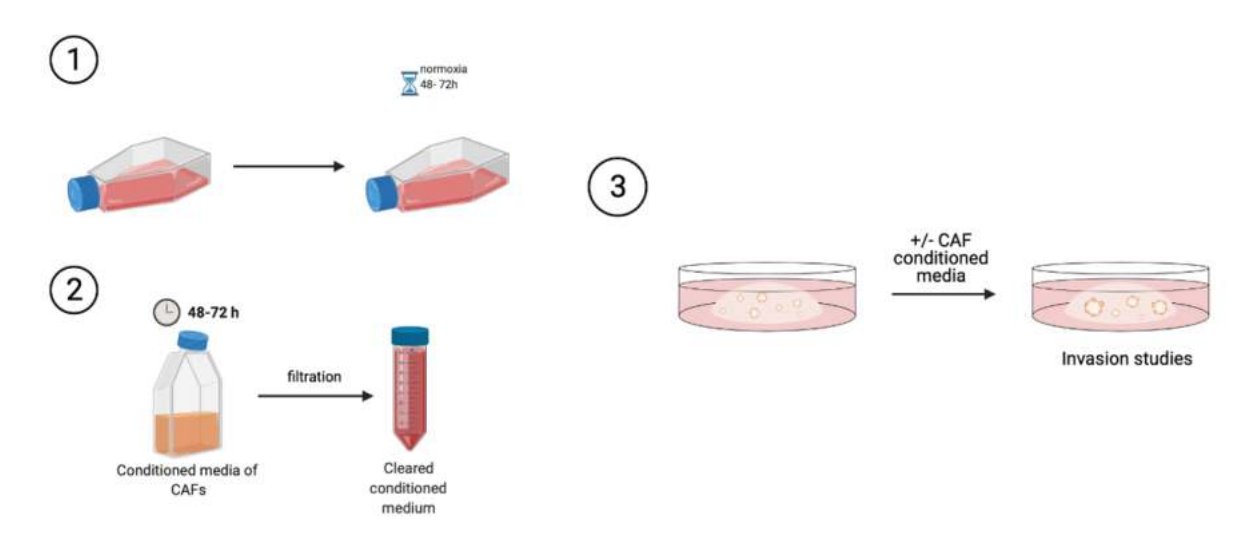
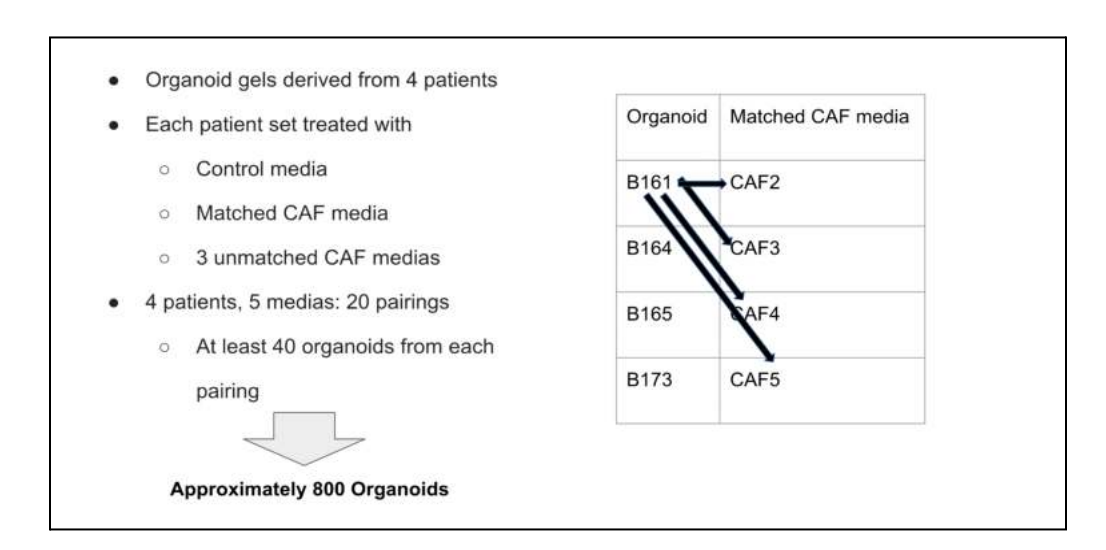


Figure 2. An outline of the procedure to make an organoid gel. From (Wood & Ewald, 2021).



**Figure 3**. The three-step procedure for making CAF-conditioned media and adding it to an already prepared organoid gel. (1) Grow CAFs (derived after cell sorting patient tumors and surrounding tissue) in culture with RPMI media (becomes CAF-conditioned media), (2) Clear the media of CAFs and debris via filtration, and (3) Add cleared media to organoid gels to test invasion. Because CAFs have been **removed** from the media permanently in step 2, only the effect of CAF-produced **substances**, **not the cells themselves**, is assessed.



**Figure 4.** Outline of how 800 organoids were chosen for analysis. Each set of patient organoids was treated with control media, its matched CAF media, and 3 unmatched CAF media.

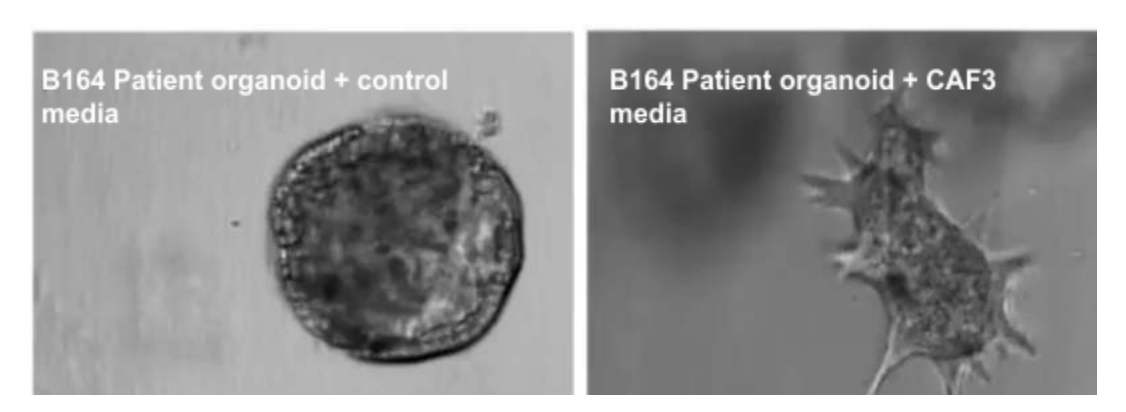


**Figure 5.** Comparison of the invasiveness (dependent variable) of an organoid treated with control media (left, independent variable) and one derived from the same patient treated with matched CAF media (right, independent variable). The organoid on the left is almost perfectly round (non-invasive); the expected circularity calculation is close to 1. The treated organoid (right) develops protrusions (invasiveness), and its circularity value is expected to be closer to zero.

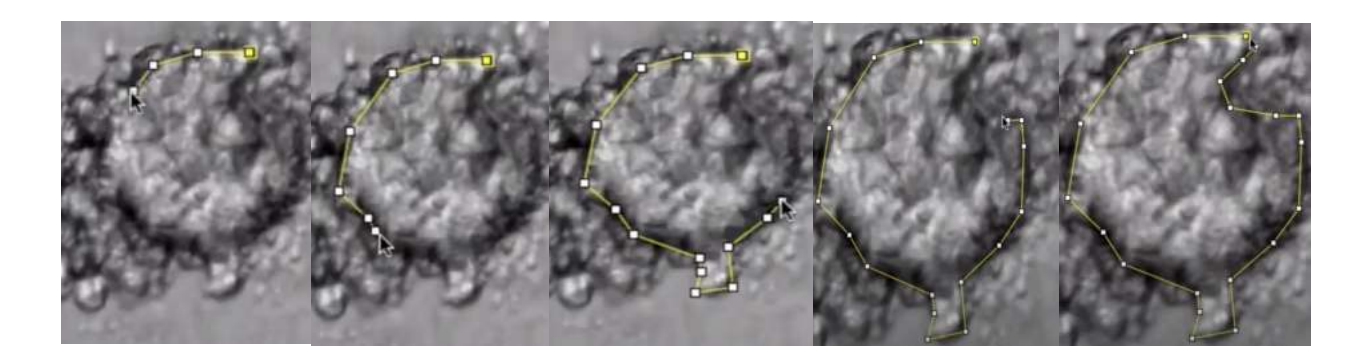


**Figure 6.** Measuring invasiveness through circularity (dependent variable) after treatment with CAF media (independent variable). These successive screenshots from a video capture the live tracing of an organoid from patient B164. The tracing produces coordinates, which get translated into a circularity value via the Fiji algorithm using the equation  $4\pi(A/P^2)$ , where A = area and P = perimeter (see (Rasband, 2017) for code).

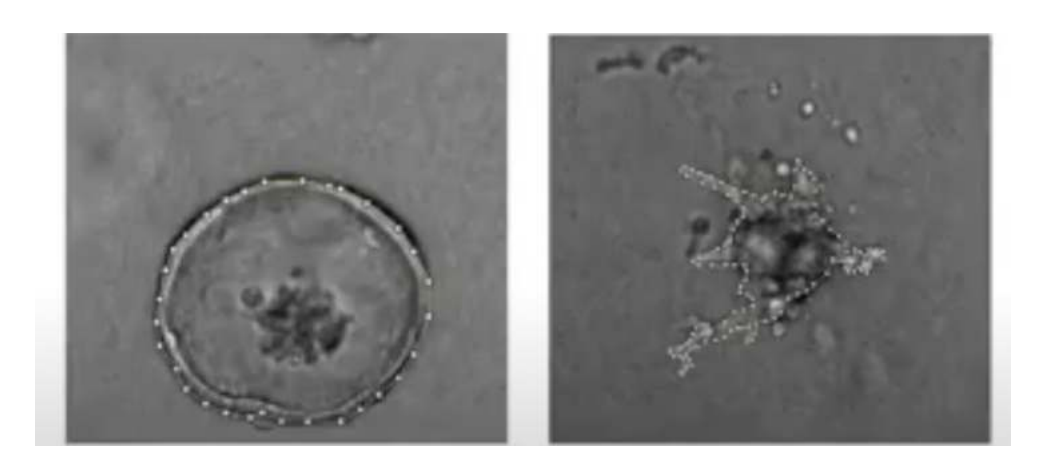


**Figure 7.** Circularity tracing (dependent variable) examples of (1) organoid from patient B165 with control media (independent variable) and (2) organoid from patient B165 with unmatched CAF media (from patient B173, independent variable). Dots around each organoid represent tracing coordinates.

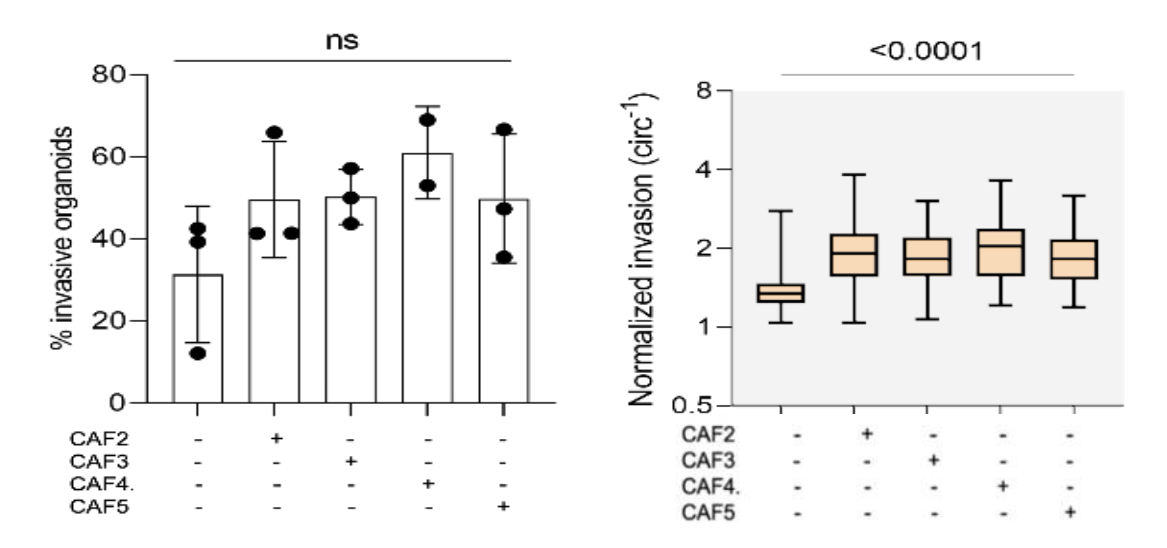


**Figure 8.** Analysis of organoid invasiveness (patient B161).

Graph 1: No statistically significant change in *percentage invasiveness* (dependent variable) among *control and CAF-conditioned media* groups (independent variable) from same and different patients (one-way ANOVA, Prism software).

Graph 2: Significant difference in the *inverse of the circularity values* (dependent variable) among these same *CAF treatment and control* groups (independent variable) (one-way ANOVA, Prism software).

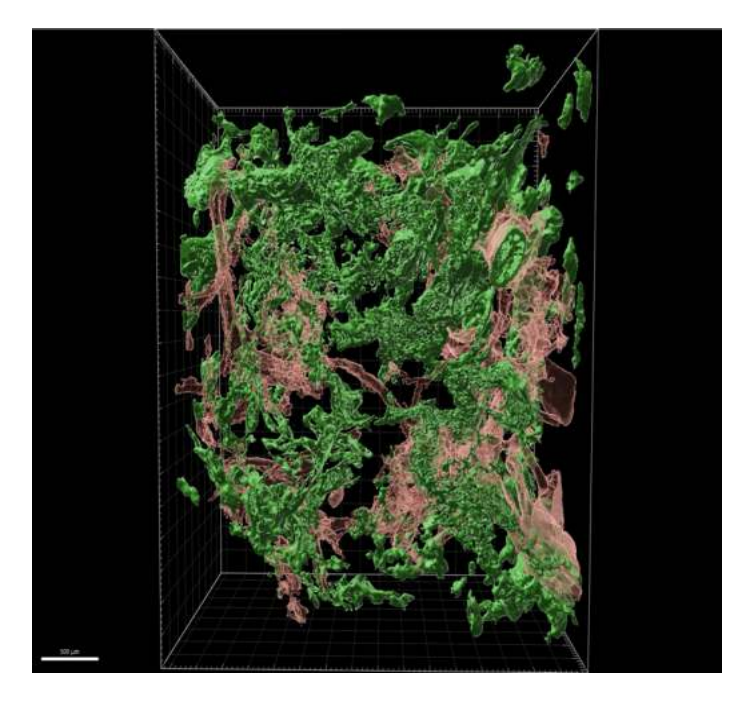
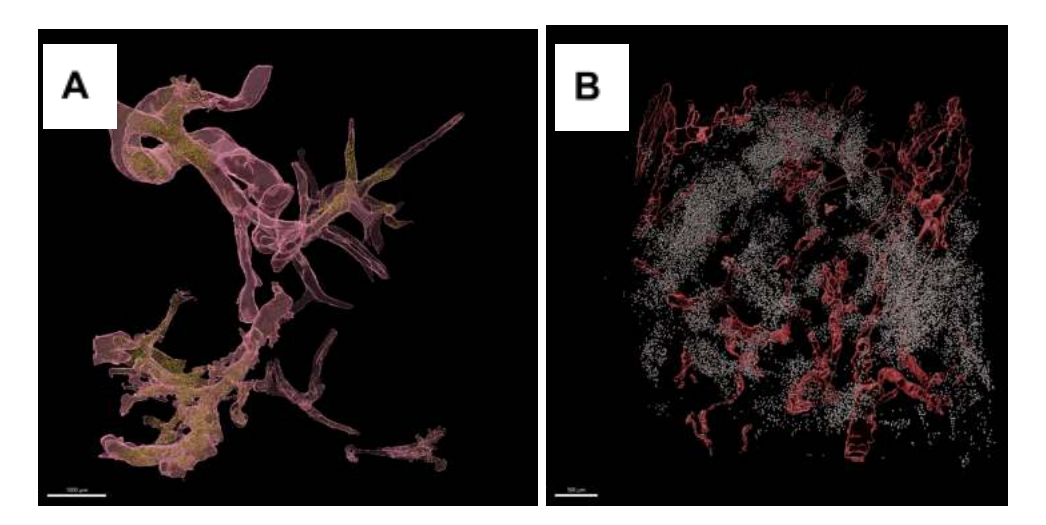
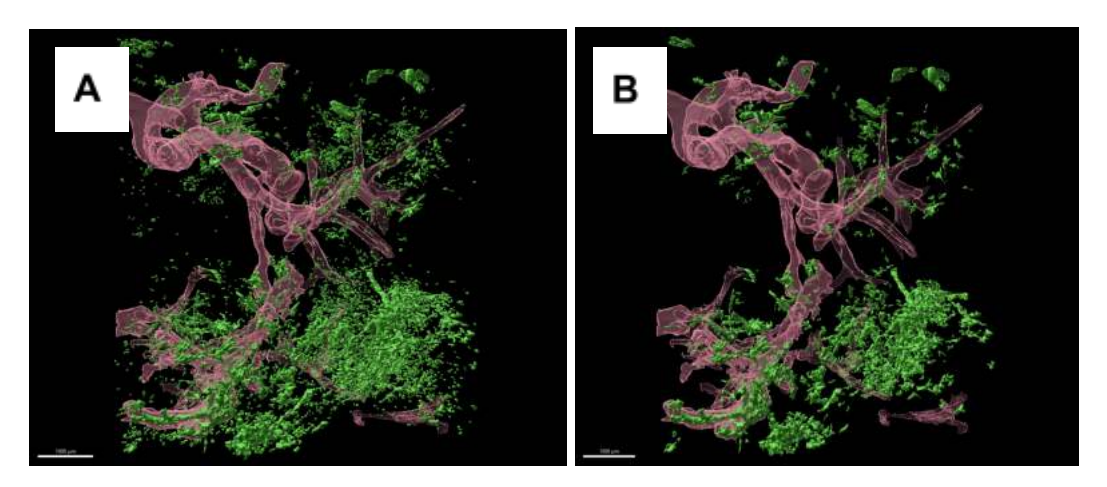


Figure 9. Example of a light-sheet microscopy 3D image of cancer after computer integration.



**Figure 10.** Effects of chemotherapy (gemcitabine/Abraxane) on tumor T42\_I. (A) Most remaining cancer (grey dots) occurs outside of the vessels (red) and in the stroma. (B) In contrast, a control tumor (cancer T44\_B) shows significant cancer mainly within vessels (yellow dots).



**Figure 11.** Examination of cancer shape in a tumor treated with chemotherapy (T44\_B). (A) This panel shows all cancer cells (green) in the background of the vessels (red). (B) Cancer growth *selected for sphericities less than 0.5*. Sphericity is a measurement of how closely a cancer gland resembles a sphere (1.0=perfect sphere, lower values indicate flattened (tubular) shapes). Comparing both figures reveals that most cancer cells have sphericities less than 0.5 (tubules, not spheres), evidenced by the fact that the two figures are very similar.